Available online at www.sciencedirect.com
ScienceDirect
C. R. Physique 10 (2009) 400–413
COMPTES RENDUS PHYSIQUE

Metamaterials / Métamateriaux

# Phase-shift, refraction and focusing based on the metamaterial technologies

Didier Lippens

*Institut d'électronique de microélectronique et de nanotechnologie, Université des sciences et technologies de Lille, UMR CNRS 8520, avenue Poincaré, BP 60069, 59652 Villeneuve d'Ascq cedex, France*

Available online 9 May 2009

**Abstract**

We address the problem of positive phase-shifting, negative refraction and focusing via a flat lens on the basis of the metamaterial technologies. With this aim, three examples are considered which differ by the technology employed and the operating frequency. The first one concerns negative-zero-positive refraction by using a prism-shaped electromagnetic metamaterial which consists of omega-type inclusion arrays operating at microwaves. The experimental verification was done in this case by angle-resolved transmission measurements. Second, we report on the phase-shift properties of a negative index transmission line which operates at Terahertz frequencies. In order to experimentally demonstrate the left-handed character of the propagation along the line, resulting in a phase advance, we used time domain experiments. At last, focusing by double refraction in a flat negative index lens was demonstrated by the theoretical and experimental mapping of the intensity of the electric field. Such a mapping of the E-field was carried out at near infrared (∼1.5 μm) by analysis in the time domain and scanning by near field optical microscopy. ***To cite this article: D. Lippens, C. R. Physique 10 (2009).***
© 2009 Académie des sciences. Published by Elsevier Masson SAS. All rights reserved.

**Résumé**

**Déphasage, réfraction et focalisation basés sur les technologies des métamatériaux.** Nous considérons les problèmes d'avance de phase, de réfraction négative et de focalisation, par lentille plane, sur la base des technologies métamatériaux. Dans ce but, trois exemples sont traités qui diffèrent par la technologie employée et la bande de fréquences de fonctionnement. Le premier exemple concerne les effets de réfraction en micro-ondes pour des valeurs d'indice négative, nulle et positive, en utilisant un prisme réalisé à partir d'inclusions en réseaux, ayant la forme omega. La vérification expérimentale est obtenue par des mesures résolues en angle de la transmission. Pour le second exemple, nous présentons les résultats des mesures de phase à la transmission pour des lignes fonctionnant aux fréquences Térahertz. Afin de démontrer expérimentalement l'avance de phase résultant du caractère main gauche de la dispersion, nous utilisons des techniques de spectroscopie dans le domaine temporel. Enfin, la focalisation par double réfraction dans une lentille plane à indice négatif est démontrée par la cartographie de l'intensité des champs électriques calculée par analyse numérique dans le domaine temporel et mesurée par des techniques de microscopie champ proche. ***Pour citer cet article : D. Lippens, C. R. Physique 10 (2009).***
© 2009 Académie des sciences. Published by Elsevier Masson SAS. All rights reserved.

*Keywords:* Negative refractive index materials; Metamaterials; Infra-red; Split ring resonators; Periodically loaded transmission line; Electro-optic sampling; Terahertz technology; Photonic crystals

*E-mail address:* Didier.lippens@iemn.univ-lille1.fr.

1631-0705/$ – see front matter © 2009 Académie des sciences. Published by Elsevier Masson SAS. All rights reserved.
doi:10.1016/j.crhy.2009.01.003

*Mots-clés :* Matériaux à indice négatif de réfraction ; Métamatériaux ; Infra-rouge, Résonateurs en anneaux ; Lignes de transmission périodiquement chargées ; Échantillonnage électro-optique ; Technologie térahertz ; Cristaux photoniques

## 1. Introduction

The number of papers devoted to electromagnetic metamaterials is now dramatically increased, with the prospect of unprecedented electromagnetic properties for the light control [1–8]. The main underlying idea of electromagnetic metamaterial technology is the achievement of an artificial magnetic dipole by taking advantage of resonant effects in the scattering of light with matter. Such resonant effects are obtained with current loops. The so-called Split Ring Resonator (SRR) scheme is probably the technology which was the most employed so far in association with wire arrays [9–11]. By this arrangement, a double negative medium can be fabricated under proper engineering rules. They based on the requirement of the overlapping of the frequency bands, where the effective permittivity and permeability are negative. Now, other types of inclusions (dielectric rods, metal clusters, ...), coupling scheme (edge- or broad-side coupled SRRs) or simply geometries (omega or S-type...) have been proposed, but the operating principles are basically the same.

On the other hand, it is well known, notably with the pioneering work of Brillouin [12] that a transmission line loaded with series capacitances and shunt inductances exhibits a high-pass filtering characteristic with a left-handed dispersion branch [13–16]. This term describes the fact the phase and group velocities show opposite directions. With respect to the refractive index, this means that the propagation of electromagnetic waves along the line is backward. The value of the effective index is negative which is equivalent to the achievement of a double negative medium.

At last, it was recently recognized that the folding of dispersion branches in the first Brillouin zone of periodic media, notably photonic crystals, yields the possibility to have also a negative value of the refractive index [17–20]. Strictly speaking this is not a metamaterial technology, which requires that the relevant dimensions, involved in the structuring of artificial matter, are much shorter than the wavelength. However, this permits one to envisage, with reasonable losses, to implement some novel applications taking benefit of a negative index in optics.

Up to now, several kinds of applications have been addressed. Their complexity greatly depends on the dimensionality and on the isotropy/anisotropy properties of the system. Focusing by a flat lens, as it was proposed by Veselago in his seminal work, was studied by many authors by taking advantage of the invariance of concepts over the electromagnetic spectrum. However, while at microwave frequencies many experimental demonstrations have been reported in the literature, any experimental demonstration in optics is still a tremendous challenge. This conclusion still holds for the superlensing effect making use of the amplification of evanescent waves. The engineering of phase or more generally of dispersion characteristics also attracted much interest with the prospect of balancing the delay in the wave propagation either by using balanced composite metamaterials or by cascading phase advanced and delayed devices. At last, it is now possible to envisage the tuning of electromagnetic properties by the inclusion of non-linear materials and devices.

In this article, we review on three examples of metamaterial technologies which were developed at the University of Lille. These examples illustrate the technologies which are currently developed at microwave, terahertz and optical frequencies. They differ by the technologies which are employed but also by the targeted applications. Therefore, while single negative refraction with a prism-like device will be considered at microwave, we will address the specific problems that an experimental demonstration of phase advance effect raise at Terahertz. Finally, double negative refraction in a photonic crystal slab will be considered.

## 2. Omega-type device at microwaves

Fig. 1(a) shows a schematic of the basic cell of the microwave prototype which consists of two back-to-back omega-type metal inclusions [21–24]. The core of the pattern is responsible for a magnetic activity through current loops via an H field excitation along the $y$ axis. The two arms of the omega pattern are responsible for the electrical activity when the electric field is polarized along the $x$ axis. Therefore, one can compare the omega patterns with the combination of SRRs (the central current loops) and wires (the arms of omega patterns). The back-to-back configuration suppresses the magneto-electric response according to the basic ideas developed in broad side coupled split ring resonators [25].

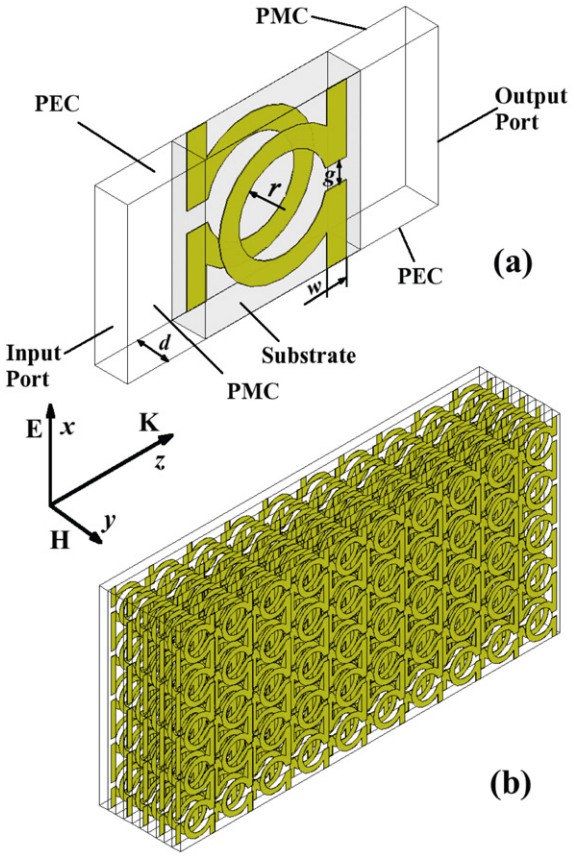


Fig. 1. Schematic of the omega-type basic cell (a) and of a slab with interconnected arms (b).

We target here to realize a negative-zero-positive metamaterials which is equivalent to a zero-gap condition between the left- and right-handed dispersion branches.

The frequency dependence of the effective permeability is governed by two characteristic frequencies of a Lorentz-like response, namely the resonant frequency of the current loop ($\omega_0$) and the magnetic plasma frequency ($\omega_{mp}$). Many experimental and theoretical works have addressed the derivation of the resonant frequencies of C- or U-shaped micro-resonators either on the basis of full wave analysis or by a lumped element approach. The latter is particularly useful in an optimization procedure notably through adjustments of substrate permittivity and thickness and metal wire width which allows one to tune easily the gap capacitance and more importantly the coupling capacitance. For this circuit-like approach, the magnetic angular resonance frequency $\omega_0$ of the current loops can be predicted by a $LC$ resonance, in which $L$ is the inductance of the current loops and $C$ is the total capacitance between the broadside coupled split ring resonators. The magnetic plasma frequency $\omega_{mp}$ is directly related to the magnetic resonant frequency $\omega_0$ and the filling factor.

The electrical response can be compared to that of an array of infinite metal wires due to the interconnected arm configuration illustrated in Fig. 1(b). In this case, the effective permittivity follows a Drude-like model and the frequency dependence of the permittivity exhibits negative values below the plasma frequency $\omega_p$. An estimate of the $\omega_p$ can be found in the seminal work of Pendry.

A zero-gap condition can be achieved when $\omega_{mp} = \omega_p$. With this aim, the degrees of freedom for a given permittivity of a substrate are the width of the metallization and the substrate thickness. In practice, the fine tuning of the balanced condition between $\omega_{mp}$ and $\omega_p$ was performed by full wave analysis (Commercial package, HFSS simulation code) of the electromagnetic behaviour of the basic cell by applying the Bloch Floquet theorem. Further details about the optimization procedure can be found in [26].

The experimental assessment of the zero-gap condition, namely the achievement of a negative-zero-positive electromagnetic medium, requires refraction experiments and thus angle-resolved transmission measurements conditions. Such experiments gives the value of the refractive index $n$ via the tracking of the refracted beam angle and the application of Snell–Descartes law either with a slab- or prism-type device. The slab shown in Fig. 1(b) cannot be used. Indeed, under tilt incidence, the incident beam experiences two refractions with a subsequent beam shift. However, the artificial medium made of a stacked omega array is highly anisotropic with a negative value of $n$ *only* in the propagation direction. This difficulty, linked to the uni-axial electromagnetic properties, can be alleviated by using a prism-type prototype.

The prism sample, composed of eleven steps was fabricated using a Printed Circuit Board technology. In practice, 0.8 mm thick epoxy substrates coated with a 35 μm copper layers ($\sigma = 5.8 \times 10^7$ S/m) were constructed according to the layout shown in Fig. 1. Owing to the large dimension of the completed prism-type prototype, we preferred to use a chemical etching technique by ferric chloride solution rather than micro milling. The number of unit cell of each layer along the propagation direction at the first and last steps was increased from five to fifteen, respectively. Each layer consists of 18 unit cells along $x$-direction with a periodicity of 3.9 mm. The variation in the number of cells is discrete, with a change of one cell by four staked layers. This corresponds to an average angle of 30.5° at the output side of the prism.

The prism refraction experimental setup consists of a parallel plate waveguide which can be compared to a scattering chamber. Two absorbing layers (Eccosorb AN-75) are used in the input section for shaping the incident beam with a quasi-plane phase front. Absorber layers were also placed around the prototype for avoiding cavity effects which could result from the reflected beams. The angle resolved measurements of the transmitted field are carried out by means of a rotating detector whose angular position is recorded via a homemade large scale circular protractor with a step of 1.25°. With respect to the similar scattering chamber which can be found in the literature, the emission as well as the detection of electromagnetic wave was performed via two horn antennas rather than by using waveguides flanges. For covering all the bands, two sets of horn pairs were used (Nadar 640 for operating in the X band and Nadar 639 for covering the Ku band). The two horns were placed at the periphery of the 96 cm-diameter aluminium plates in order to satisfy the far field condition. The refraction measurement was performed by a HP 85107A Vector Network Analyzer.

Prior to the refraction experiments we performed ab initio calculations by a proper representation of the microstructure rather assuming that the prism behaves as an effective homogeneous medium. Figs. 2(a), (b) and (c) show the maps of the electric field magnitude at various operating frequencies calculated at the mid-plane between the top and bottom perfect electric conductors. The black arrow and the dash-dot line indicate the direction of the refracted beam and the normal to the second tilted interface, respectively. For a frequency of 10.0 GHz (Fig. 2(a)), it can be seen that the angle of the refracted beam is in the negative direction with respect to the normal as expected for a left-handed dispersion branch. At 12.8 GHz (Fig. 2(b)), the refracted beam direction is quasi-parallel to the normal, indicating that the refractive index is extremely close to zero. The magnitude of the refracted beams at 12.8 GHz and 10.0 GHz are comparable. Finally at 15 GHz (Fig. 2(c)) the peak of refracted beam is directed along a positive angle with respect to the normal and is consistent with a right-handed branch.

Fig. 3(a) shows a photo of the prism and 3(b) illustrates the results of experiments. The latter shows the normalized intensity of the refracted beam as a function of angular position of the probing horn antenna for three characteristics frequencies corresponding to a negative, zero and positive index. By taking the central angle at the full width at half maximum, the refraction beam peak was found to occur at −38.0°, 0.5° and 13.0°, at 11.1 GHz, 13.6 GHz and 15.0 GHz, respectively. Moreover, half beam width of the refracted beam is only 15.9° at 13.5 GHz, which is smaller than that of 18.2° at 15.0 GHz and 29.2° at 11.1 GHz, consistent with the unique characteristics of a zero index metamaterial.

The frequency dependence of the refractive index, computed from the Snell–Descartes' law, is plotted in Fig. 4(a). We see that the increase in the refractive index with frequency is continuous throughout the negative index to the positive index region. Thus, the experimental result demonstrates that the proposed structure indeed exhibits a balanced property with a negative-zero-positive behaviour. The slight shift of the transition frequency between the experimental and numerical retrieved results is mainly due to the substrate permittivity lower in the simulation. However, it is noted that the balanced condition is sustained because it does not depend on the substrate permittivity. Furthermore, the group velocity $v_g$ of this metamaterial can also be obtained from the phase index $Re(n)$ as follows.

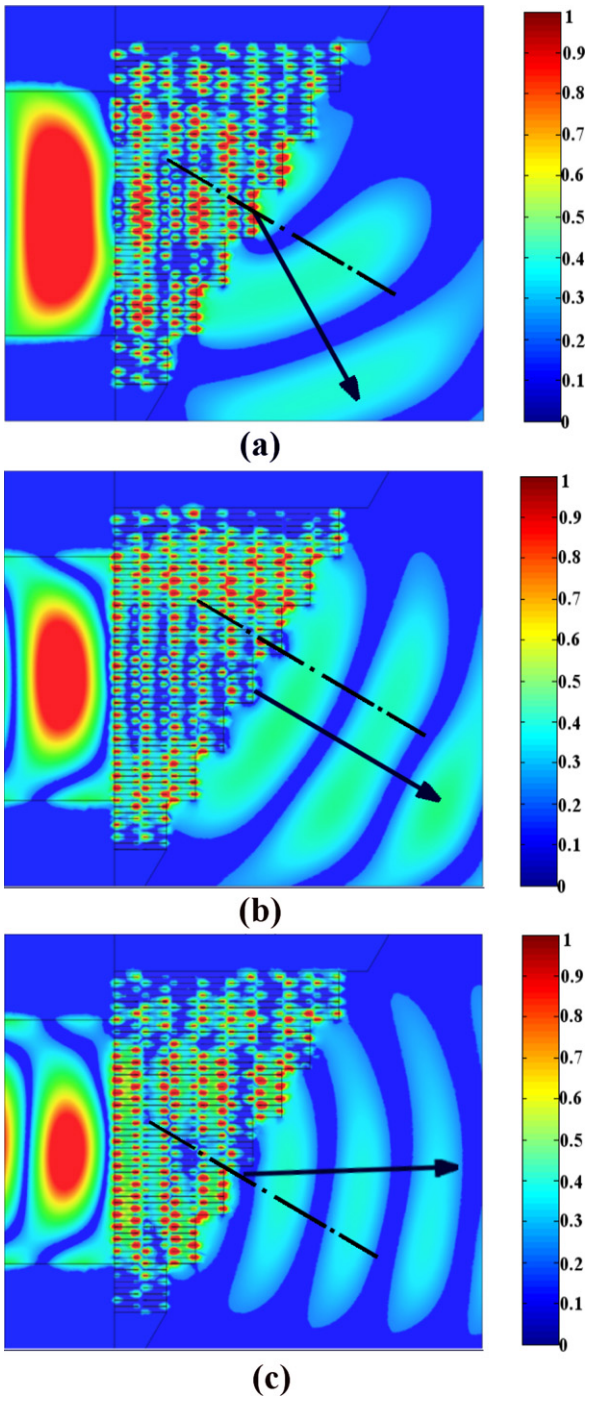


Fig. 2. Electric field magnitude of refracted beam at different frequencies, (a) 10.0 GHz, (b) 12.8 GHz, (c) 15.0 GHz.

$$v_g = \frac{c}{Re}(n) + \omega \frac{\partial Re(n)}{\partial \omega}.$$

As shown in Fig. 4(b), the group velocity continuously decreases as the frequency is increased, indicating that the proposed structure is highly dispersive. For the transition frequency of 13.6 GHz, the group velocity is $4.8 \times 10^7$ m s$^{-1}$. This result clearly shows that energy can be transmitted through the device and offers possibility to make use of the desired frequency point of zero refractive index. The high dispersive characteristics which were just demonstrated

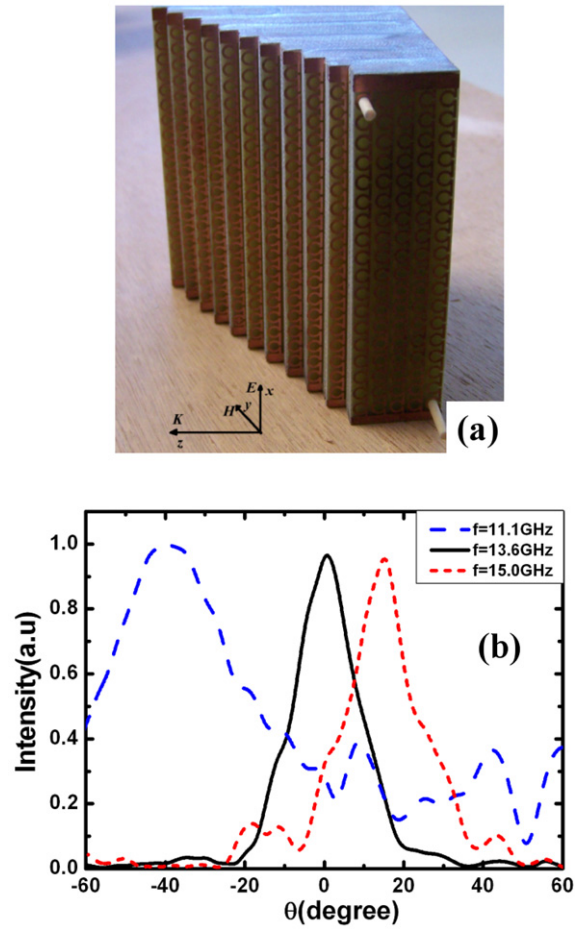


Fig. 3. Photo of the prism-like prototype (a) measured.

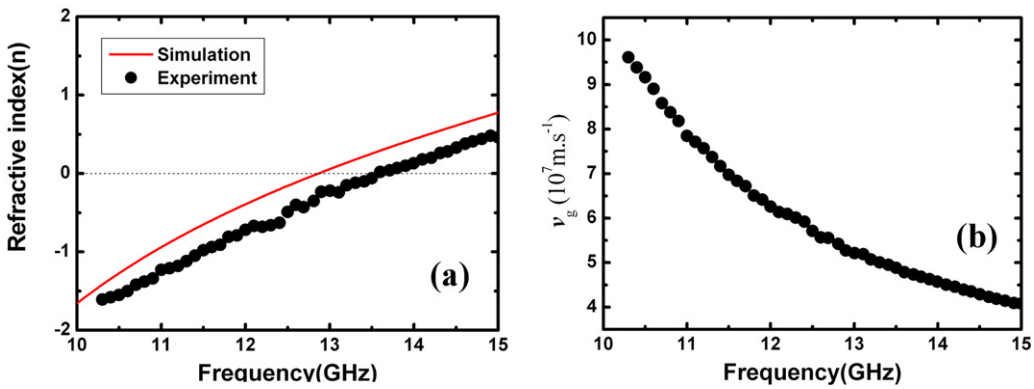


Fig. 4. (a) Refractive index as a function of frequency. (b) Frequency dependence of the group velocity.

experimentally along with a non-vanishing group velocity could find many applications, notably for rainbow-type devices. In fact, it is well known that the dispersion of the refractive index in a prism-like device yields a decomposition of the different frequency components of an incident light. The study reported here is based on the same underlying idea by taking benefit of the emerging metamaterial technology.

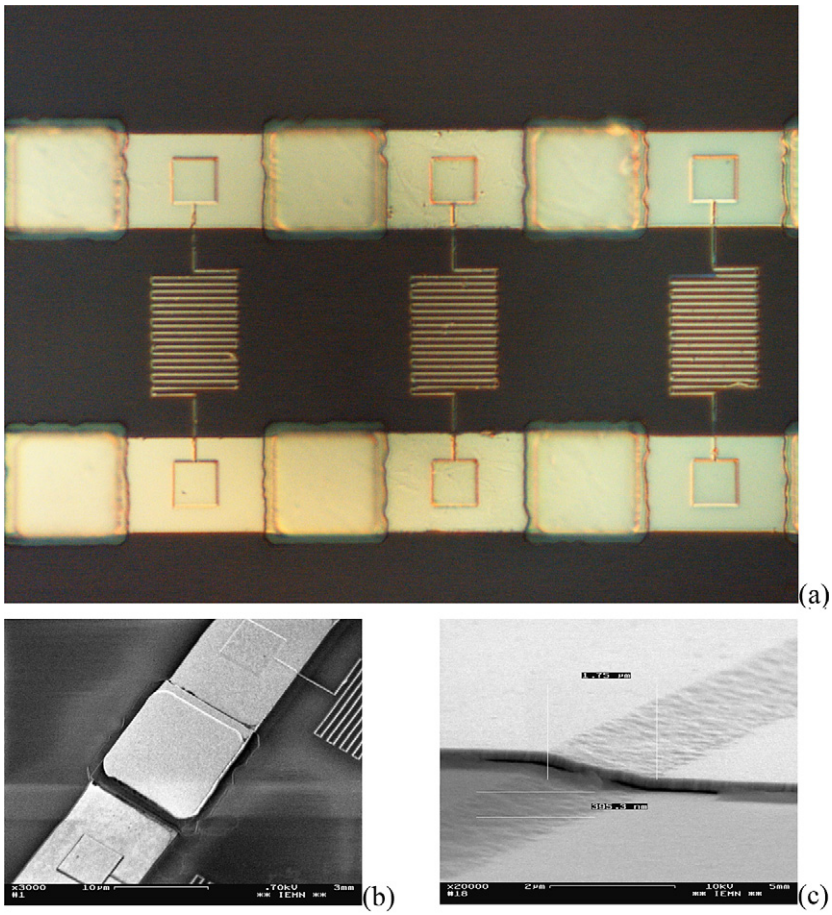


Fig. 5. Photo of a THz periodically loaded transmission line (a) and illustration of the technologies (b), (c).

## 3. Left-handed transmission line at Terahertz frequency

Let us consider now the possibilities afforded by a transmission line approach. This approach was widely used at microwaves for implementing many novel applications or simply for the miniaturization of guiding and radiating elements which can be scaled on a dimension shorter than the wavelength. In this section, we study how such an approach can be extended at higher frequencies notably at Terahertz frequencies. The underlying idea for implementing a left-handed propagation medium is the same, namely the loading of a transmission line by series capacitances and shunt inductances. Only the technology changes. In addition due to the lack of vectorial continuous wave analyzers at Terahertz frequency we show how a coherent Time Domain Spectroscopy (TDS) technique allows one to point out the left-handedness of dispersion characteristics.

Fig. 5 is an optical view of the left-handed transmission lines characterized in the present work. For the sake of simplicity in the integration of the lumped reactive elements, we chose a Co-Planar Strip (CPS) configuration. The width of the metal strip is 10 μm while the slot between the two lines is 25 μm. With this configuration, it can be shown that the problems in connection with surface shock waves can be alleviated. The characteristic impedance of the bare line is calculated to be 160 Ω. For observing backward propagation, the lines have to be periodically loaded by series capacitances and by shunt inductances as aforementioned. In order to succeed in the fabrication of the self inductance with dimensions on a deep submicron scale, electron-beam patterning of PMMA resists was used while the $Si_3N_4$ layer deposition was performed by Plasma Enhanced Chemical Vapour Deposition (PECVD). Titanium/Gold metal layers were deposited for the fabrication of strips and pads by means of an electron gun evaporator. The thickness of gold is typically 280 nm for a Titanium thickness of 20 nm. Fig. 5(b) and (c) illustrate the nanotechnologies employed

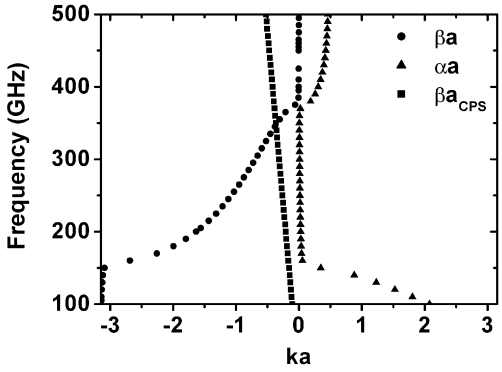


Fig. 6. Dispersion characteristics of the transmission line loaded by series capacitances and shunt inductances.

with a close view by scanning electron micrograph of the capacitance edge showing the dielectric cross-over and of the pinning of the meander-like inductance to the strip line.

In practice, the design of these various elements was carried out by the calculation of the dispersion characteristics and reverse engineering targeting an operating window above 100 GHz. To this aim, we use the procedure that we already applied in a previous work for the derivation of the band diagram of metamaterial waveguide structures [27]. In short, we calculate by full wave analysis the scattering parameters of a unit cell. We then convert the scattering $S_{ij}$ matrix of this unit cell in a chain matrix which is compared to the one of a homogeneous transmission line, characterized by its propagation constant $\gamma = \alpha + j\beta$.

In Fig. 6, we plotted the results of this calculation for a bare CPS line for positive $k$ and for the periodically loaded line. For negative value of $k$, the dispersion branch is left-handed. Therefore, the periodically transmission line exhibits a pass band transmission characteristics with an ultra-wide forbidden gap at low frequency up to 150 GHz (imaginary values of the $k$ vector) and above 350 GHz. In order to characterize experimentally the dispersion above 100 GHz (in practice many commercial vectorial network analyzers are frequency limited to 110 GHz), we used a TDS technique taking advantage of the recent progress in ultra-fast semiconductor switching devices.

The basic idea is to convert an ultra-short optical pulse delivered by a femtosecond laser into an ultra-short electrical pulse [28–30]. Under this condition, the spectral content of the electrical pulse reaches the Terahertz spectral region and the transmission properties of the line can be assessed. However, the magnitude as well as the phase-shift of the transmission through the line have to be recorded as a function of frequency. Such a requirement can be satisfied with the so-called pump-probe experimental set up. In short, the recording of the electrical pulse excitation, as well of the transmitted and reflected pulses, are carried by using the same laser source, thus keeping the phase coherence. On the other hand, the assessment of the left-handed character of the wave propagation on the line needs to carry out a differential phase measurement between two lines with different lengths.

In practice, for the excitation of ultra-short pulses we used a low temperature grown AlGaAs technology. By varying the aluminium concentration, the absorption band edge can be tailored so that a GaAs LTG layer transforms the optical pulse into an electrical one by photo-doping. On the other hand, the introduction of a low concentration of Aluminium shifts the absorption characteristics so that the is the creation of electron hole pair can be monitored by the electric field of the pulse. This assisted absorption mechanism is known as the Franz Keldysh effect. Fig. 7 illustrates the various issues for comparing the phase-offset between a 17 and 21 cell transmission line.

Initially, the lines are 2 mm long with two $100 \times 100$ μm$^2$ pads at the ends in order to bias the semi-conductor patches at a relatively dc high voltage ($\sim 60$ V) for observing the modulation of the assisted absorption by Franz Keldysh effect. In order to probe the transmitted electromagnetic waves as well as the reflected ones, LT GaAs films have been wafer bonded in the input (only the edge of the patches are apparent on the photo) and an AlGaAs thin layer in the output port of the line. In addition, these semi-conductor 'patches' overlap two adjacent lines The adjacent lines have a various number of unit cell so that differential phase measurement can be carried out.

Fig. 8 shows the typical time variations of the signals recorded at the output port of a 17 cells and 21 cells line. The time scale involved in the time variations of the transmitted signal is around 3 ps thus corresponding to a characteristic frequency around 300 GHz. As expected, it can be seen that the line behaves as a band pass filter at millimetre and sub-millimetre wavelengths in agreement with the dispersion characteristic shown in Fig. 6. Indeed, the stop bands below

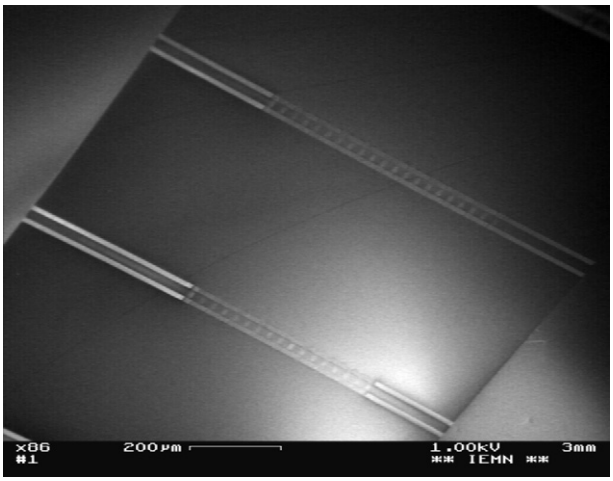


Fig. 7. Scanning Electron micrograph of 17 and 21 cell transmission lines.

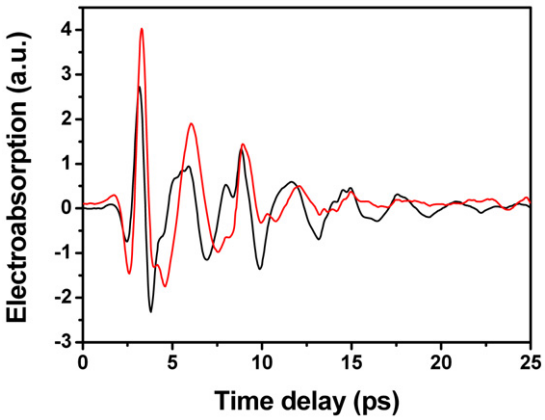


Fig. 8. Time dependence of the transmitted signal.

100 GHz and in the frequency band above 350 GHz select the frequency components of the Fourier transform of the initial pulse. The transmitted signal shows an oscillating form in contrast to the incident pulse. These first conclusions drawn from the time analysis can be confirmed by calculating the Fourier Transform of incident and transmitted signals which are reported in reference [31] where further details can be found. While the spectrum of the input signal extends well above 1 THz, the spectral density of the transmitted one shows a well defined pass band which fits, with a reasonable agreement, the band calculated by full-wave simulation. The maximum in the spectral density is achieved for 340 GHz for a 3 dB bandwidth of 90 GHz. We thus obtained experimentally a relative bandwidth around 25%.

At this stage, it is interesting to see whether quantitative measurements can be performed in order to determine the losses along the line. A 10 dB loss level has been estimated at 340 GHz from the Fourier transforms. This corresponds to a 0.6 dB of loss per unit cell if we are considering the losses mainly due to the left-handed cells. Such a level is reasonable and can be compared to the lowest published so far for metamaterial propagation media.

The good fit between the calculated left-handed dispersion branch and the Fourier transform of the time dependence of the transmitted signal is a first indication of a backward wave propagation mode along the line. However, direct evidence is possible due to the fact the line stops most of the low frequency Fourier components (below 100 GHz) which are the most intense in the spectral density of the incident pulse. In contrast those corresponding to the high frequency side are either stopped or would be transmitted via the right-handed branch above 800 GHz of minor importance. This permits us to have a direct clue to left-handedness by measuring phase advance in the signal transmitted by two lines which differ by the number of cells. By considering in Fig. 8, it can be noticed that

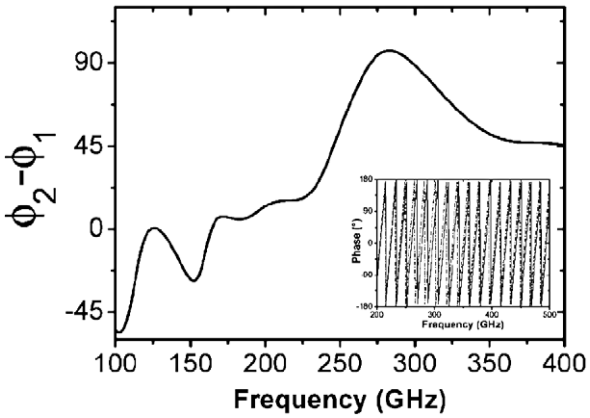


Fig. 9. Frequency dependence of the phase-offset between two lines.

the transmitted signal for the 21-cells line shows a phase advance with respect to the 17-cells one confirming experimentally the left-handed behaviour of the transmission line. Fig. 9 shows the phase difference of the two signals ($\Delta\Phi = \Phi_{21\ \text{cells}}(f) - \Phi_{17\ \text{cells}}(f)$) which can be plotted after Fourier transform: The positive phase offset found here support the idea of backward wave propagation over the bandwidth where $v_p \cdot v_g < 0$, where $v_p$ and $v_g$ are the phase and group velocities, respectively.

The potential applications of the left-handed transmission lines are numerous as briefly discussed in the introduction. The geat majority so far concern linear applications by taking benefit of the reversal of the phase velocity with respect to the group one. Also, it is believed that one of the promising applications would be non-linear photonics notably harmonic conversion and parametric amplification.

## 4. Photonic crystal flat lens at NIR

Let us now consider the negative index material technology which could be employed in optics and especially at the wavelength of telecommunications systems ($\lambda = 1.5$ μm). In the literature there are considerable efforts in order to extend the basic concepts of double negative media via the fabrication of current loops [32,33] or for developing transmission line approaches which are extended to 2D or 3D photonics systems.

Metallo-dielectric would be a suitable solution for satisfying the metamaterial condition. However, negative refraction was demonstrated by using a photonic crystal approach [34–36]. By the use of a full dielectric approach, lower losses than those demonstrated with metal based nanostructures can be expected. In counterpart whereas focusing by means of a flat lens is here verified experimentally, the resolution is on the wavelength scale as expected by the diffraction limited operating regime.

Fig. 10 illustrates how a negative refraction mode can be achieved with photonic crystals by the plotting of the dispersion diagram. This figure shows the typical TE and TM band diagrams of 2D PCs consisting in a triangular lattice of air holes etched in a dielectric slab with an air filling factor of 38%. A slab effective index value of 3.26 was taken into account and corresponds to the effective index of the fundamental guided mode supported by a layered InP/GaInAsP/InP semiconductor heterostructure for insuring the light confinement along the growth direction. The negative refraction regimes can occur within two ranges of wavelength. This can be achieved first for both TE and TM fundamental band near $a/\lambda = 0.23$ around the K point of the first Brillouin zone. In this regime, the refractive index is positive but it has been shown that group and phase velocities can be of opposite sign leading also to focusing with a PC slab. Second, a negative refraction index can be obtained for the TE second band ($0.23 < a/\lambda < 0.36$). In this range, the PC is opaque for TM waves. In contrast, the TE second band exhibits a negative slope everywhere and the wavevector isotropy is relatively preserved, as shown by the circular iso-frequency contours. Further details about these calculations can be found in [37]. Under these conditions, a negative index can be defined and the value of $n = -1$ is achieved as the light line crosses the second band. Thus in order to realize a lens operating at 1.55 μm, the lattice constant of the 2D PCs must be adjusted to 476 nm with a hole diameter of 350 nm. Such configuration corresponds to $a/\lambda = 0.307$.

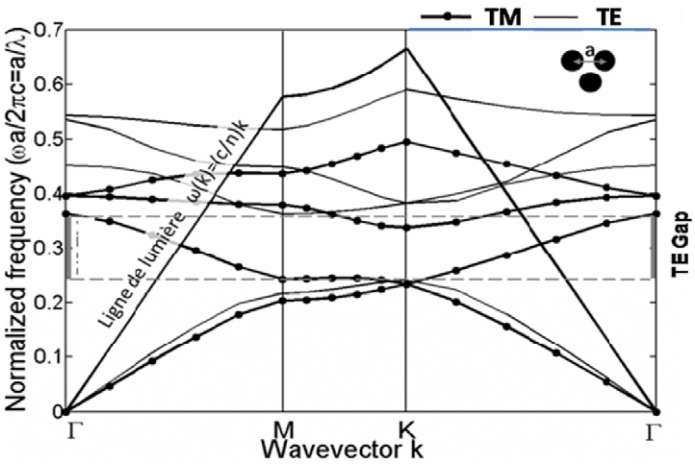


Fig. 10. 10 band structure of a triangular hole arrays in an InP substrate.

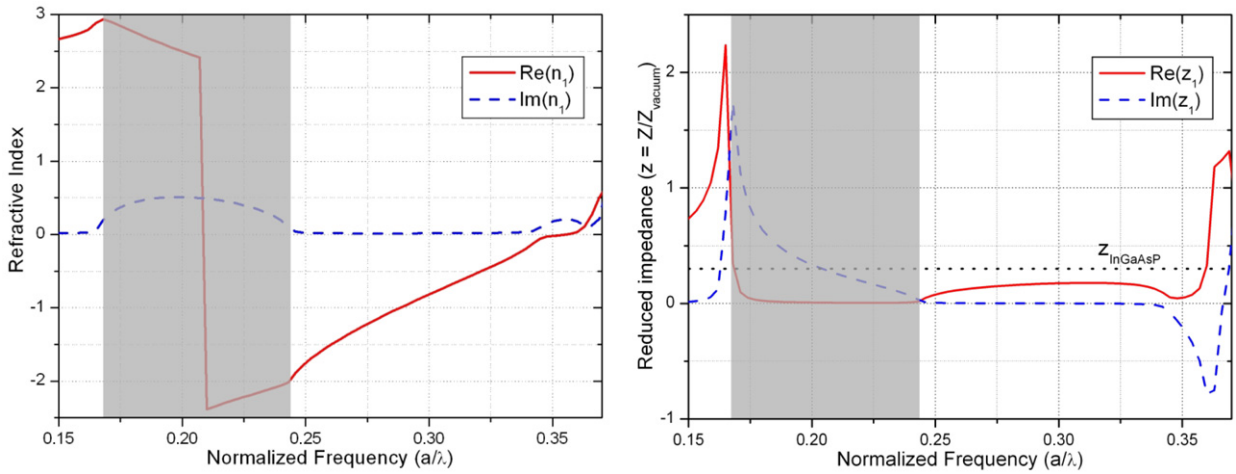


Fig. 11. Illustration of impedance and index matching issues.

Before considering the fabrication, it is worth-mentioning that the matching of the refractive index is a necessary condition, but is not sufficient [38]. In fact, impedance matching is also required, which is far from being a simple task. In order to illustrate this issue we plotted in Fig. 11, the frequency dependence of the effective index and of the characteristic impedance of typical PC in the frequency band of interest. For the sake of simplicity in the retrieval of the effective parameters via a Fresnel inversion technique [39], we assumed here a square lattice but the conclusions drawn here are still valid for a triangular lattice. While a matching of the index is met, at the centre frequency, it can be noticed that the characteristic impedance over the second band is limited by the impedance of the confinement InGaAsP semiconductor layer.

Fig. 12(a) shows a photo of the PC flat lens which was fabricated whereas Fig. 12(b) illustrates the SNOM experiment which were carried at the University of Bourgogne in De Fornel's research group. The 2D photonic crystal slab was made of deep etched holes with a triangular lattice. Also, the manufacturing stage also involves the fabrication of a quasi-point source by means of a truncated ridge waveguide, placed in front of a flat lens. The general scheme in order to fabricate the lens consists of three major stages: (i) the growth of the three layered confinement epilayer by gas source molecular beam epitaxy; (ii) the nanoscale patterning by e-beam lithography using in the present process HSQ electron sensible resist; and (iii) the fabrication of hole array along with the ridge waveguide by induced couple plasma (ICP) etching. Further details about the design and technological issues can be found in Ref. [40].

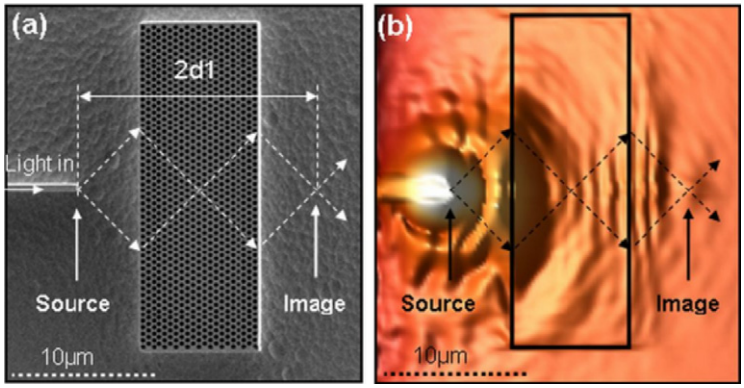


Fig. 12. Scanning Electron Micrograph of a photonic crystal flat lens (a) and map of the electric field intensity by SNOM (b).

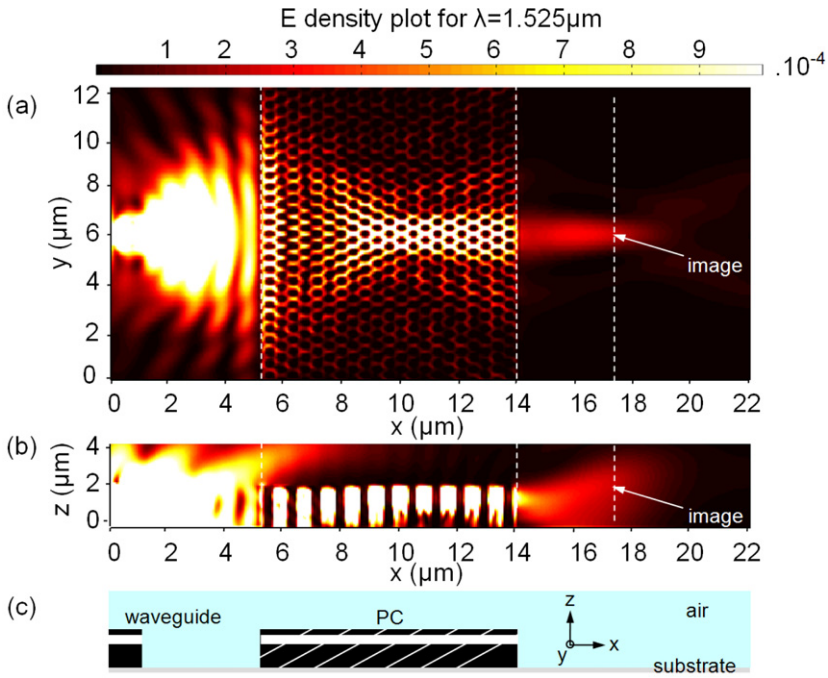


Fig. 13. 3D simulation of a Flat PC lens (a) top view (b) cross section and (c) schematic of the device under test.

At this stage, it seems interesting to see the information which could be drawn from ray-tracing as it was made in the original work of Veselago. Fig. 12 illustrates such an approach. It can be shown that the positions of various foci are in agreement with Snell–Descartes Law for a refractive index which is negative with a value close to $n = -1$.

The ray tracing approach which have been used above gives some qualitative arguments in favour of the successful demonstration of negative refraction using PC with negative index close to one. Further information about the resolution and of the level of transmission can be achieved by means of three-dimensional simulations [41] which are now possible thanks to the recent progress in modelling resources. The results of a three-dimensional simulation are displayed in Fig. 13. A bright spot is seen in the input section as a direct consequence of the high impedance mismatch between air and the characteristic impedance of the PC structure. A clear focus located approximately at the middle of the PC slab is also clearly apparent. The second focus on the output section is more difficult to localize because this is the intensity of the electric field which is here displayed. Presumably due to the mismatch pointed out before, the focus exhibits an oblong shape. Whereas some waist can be defined within the lens approximately in the middle, it seems however that the maximum of the intensity of the transmitted light is located at a shortest distance with respect

to the focal plane (dashed line in the output section). From the intensity mapping displayed in Fig. 13(b) it can be seen that the light which is radiated from the lens shows a relatively complex radiation pattern in the near field region so that the interpretation is difficult.

Finally, let us discuss the ability to produce a sub-wavelength image of the source point as proposed in Pendry work. In order to evaluate the Full Width at Half Maximum (FWHM) of the focused spot, a Gaussian fit of the transverse cross-section of the spot along the *y* direction was used. For wavelengths ranging from 1510 nm to 1540 nm, the spot FWHM values are dispersed between $\lambda_0$ and $1.2\lambda_0$ where $\lambda_0$ is the free space wavelength. The SNOM measurements enlarge this value due to the finite size of the SNOM probe ($\sim$100 nm) [42]. As a consequence, the real FWHM is lower than the measured one. In conclusion, PC flat lenses which are based on the reversal of the curvature of the second dispersion branch can be useful in focusing application by taking advantage of the invariance of phenomena by translating the source in a parallel direction to the interfaces. The achievement to overcome the Raleigh limit is however problematic owing to structuring on a scale comparable to the wavelength.

## 5. Conclusion and prospects

Metamaterial technologies are now attracting much interest with first principles proofs in optics to some demonstrations very close to the applications at microwave. The applications describe in this review paper concern negative index materials. It is believed that many other applications can be addressed owing to the opening of the effective parameter space. Frequency selective surfaces which exhibit a deep rejection in the transmission spectrum, hyperlensing by tailoring the permittivity tensor or cloaking by introducing radial or tangential gradients of permittivity or permeability are among the most promising applications today [43–46]. At last, the tunability of the dispersion characteristics can be envisaged either by a ferroelectrics or liquid crystal technology [47].

## Acknowledgements

I would like to thank all the members of the DOME group, notably Fuli Zhang for the results demonstrated for the negative-zero-positive metamaterial, Thomas Crespin for the study of the THz left-handed transmission line and Nathalie Fabre along with Charles Croënne for their work on focusing via a flat PC lens. The authors would like also to thank his colleagues Olivier Vanbésien, Eric Lheurette, Xavier Mélique and Véronique Sadaune from DOME group along Jean François Lampin and Ludovic Desplanque from epitaxy group at IEMN for their contribution to this work. Also, many thanks are givent to Benoit Cluzel and Frédéric De Fornel from the University of Bourgogne (Dijon). Their help was determinant for the SNOM experiments carried out on PC flat lenses. This work was carried out in the framework of CNES (Centre National d'Etudes Spatiales), of DGA (Délégation générale à l'armement) and ESA (European Space Agency) contracts on metamaterial technologies.

## References

[1] V.G. Veselago, Sov. Phys. Usp. 10 (1968) 509.
[2] V.G. Veselago, Some remarks regarding electrodynamics of materials with negative refraction, Appl. Phys. B 81 (2005) 403.
[3] J.B. Pendry, A.J. Holden, D.J. Ribbins, W.J. Stewart, IEEE Trans. Microwave Theory Tech. 47 (1999) 2075.
[4] J.B. Pendry, A.J. Holden, W.J. Stewart, I. Youngs, Phys. Rev. Lett. 76 (1996) 4773.
[5] J.B. Pendry, Phys. Rev. Lett. 85 (2000) 3966.
[6] A. Grbic, G.V. Eleftheriades, Phys. Rev. Lett. 92 (2004) 117403.
[7] R. Shelby, D.R. Smith, S. Schultz, Science 292 (2001) 77.
[8] D.R. Smith, W.J. Padilla, D.C. Vier, S.C. Nemat-Nasser, S. Schultz, Phys. Rev. Lett. 84 (2000) 4184.
[9] R.A. Shelby, D.R. Smith, S.C. Nemat-Nasser, S. Schultz, Appl. Phys. Lett. 78 (2001) 489.
[10] S. Enoch, G. Tayeb, P. Sabouroux, N. Guérin, P. Vincent, Phys. Rev. Lett. 89 (2002) 213902.
[11] D.R. Smith, D.C. Vier, T. Koschny, C.M. Soukoulis, Phys. Rev. E 71 (2004) 036617.
[12] L. Brillouin, Wave Propagation and Group Velocity, Academic, New York, 1960.
[13] A. Lai, C. Caloz, T. Itoh, IEEE Microwave Mag. 5 (2004) 34.
[14] S. Lim, C. Caloz, T. Itoh, IEEE Trans. Microwave Theory Tech. 53 (2004) 161.
[15] A. Lai, C. Caloz, T. Itoh, IEEE Microwave Wireless Components Lett. 14 (2004) 68.
[16] M. Antoniades, G. Eleftheriades, Antennas and Wireless Propagation Lett. 2 (2003) 103.
[17] M. Notomi, Phys. Rev. Lett. B 62 (2000) 10696.
[18] C. Luo, S.G. Jonhson, J.D. Joannopoulos, J.B. Pendry, Phys. Rev. Lett. B 62 (2002) 201104.

[19] C. Luo, S.G. Jonhson, J.D. Joannopoulos, J.B. Pendry, Phys. Rev. Lett. B 68 (2003) 045115.
[20] P.V. Parimi, W.T. Lu, P. Vodo, J. Sokoloff, J.S. Derov, S. Sridhar, Phys. Rev. Lett. 92 (2004) 127401.
[21] J. Huangfu, L. Ran, H. Chen, X. Zhang, K. Chen, T.M. Grzegorczyk, J.A. Kong, Appl. Phys. Lett. 84 (2004) 1537.
[22] L. Ran, J. Huangfu, H. Chen, Y. Li, X. Zhang, K. Chen, J.A. Kong, Phys. Rev. B 70 (2004) 073102.
[23] L. Ran, J. Huangfu, H. Chen, X. Zhang, K. Cheng, T.M. Grzegorczyk, J.A. Kong, Prog. Electromagn. Res. 51 (2005) 249.
[24] E. Lheurette, O. Vanbésien, D. Lippens, Microwave Opt. Tech. Lett. 49 (2007) 84.
[25] R. Marques, F. Mesa, J. Martel, F. Medina, IEEE Trans. Antennas Propag. 51 (2003) 2572.
[26] F. Zhang, G. Houzet, E. Lheurette, X. Zhao, M. Chaubet, D. Lippens, J. Appl. Phys. 75 (2007) 195111.
[27] T. Decoopman, O. Vanbesien, D. Lippens, IEEE Microwave Wireless Components Lett. 14 (2004) 507.
[28] L. Desplanque, J.F. Lampin, F. Mollot, Appl. Phys. Lett. 84 (2004) 2049.
[29] J.F. Lampin, L. Desplanque, F. Mollot, Appl. Phys. Lett. 78 (2001) 4103.
[30] L. Desplanque, E. Peytavit, J.F. Lampin, D. Lippens, F. Mollot, Appl. Phys. Lett. 83 (2003) 2483.
[31] T. Crépin, J.F. Lampin, T. Decoopman, X. Mélique, L. Desplanque, D. Lippens, Appl. Phys. Lett. 87 (2005) 104105.
[32] G. Dolling, M. Wegener, C.M. Soukoulis, S. Linden, Opt. Lett. 32 (2007) 53.
[33] K. Aydin, I. Bulu, E. Ozbay, Appl. Phys. Lett. 90 (2007) 254102.
[34] A. Berrier, M. Mulot, M. Swillo, M. Qiu, L. Thylen, A. Talneau, S. Anand, Phys. Rev. Lett. 93 (2004) 073902.
[35] E. Schonbrun, T. Yamashita, W. Park, C.J. Summers, Phys. Rev. B 73 (2006) 195117.
[36] T. Matsumoto, K. Eom, T. Baba, Opt. Lett. 31 (2006) 2786–2788.
[37] M. Perrin, S. Fasquel, T. Decoopman, M.X. Mélique, O. Vanbésien, E. Lheurette, D. Lippens, J. Opt. A: Pure Appl. Opt. 7 (2) (2005) S3–11.
[38] D. Maystre, S. Enoch, J. Opt. Soc. Amer. A 21 (2004) 122–131.
[39] C. Croenne, N. Fabre, D.P. Gaillot, O. Vanbésien, D. Lippens, Phys. Rev. B 77 (2008) 1.
[40] N. Fabre, S. Fasquel, C. Legrand, X. Mélique, M. Muller, M. François, O. Vanbésien, D. Lippens, Opto-Electronics Rev. 14 (2006) 225.
[41] N. Fabre, X. Mélique, D. Lippens, O. Vanbésien, Optimized focusing properties of photonic crystal slabs, Opt. Commun. 281 (13) (2008) 3571.
[42] B. Cluzel, D. Gérard, E. Picard, T. Charvolin, F. de Fornel, E. Hadji, J. Appl. Phys. 98 (2005) 86109.
[43] H.T. Chen, J. O'Hara, A.K. Azad, A.J. Taylor, R.D. Averitt, D.B. Shrekenhamer, W.J. Padilla, Nature Photonics 2 (2008) 295.
[44] H. T Chen, W. Padilla, J.M.O. Zide, S.R. Bank, A.C. Gossard, A.J. Taylor, R.D. Averitt, Opt. Lett. 32 (2007) 1620.
[45] D. Gaillot, C. Croënne, D. Lippens, A full dielectric route for Terahertz cloaking, Opt. Express 16 (2008) 3986.
[46] O. Vanbésien, N. Fabre, X. Mélique, D. Lippens, Appl. Opt. 47 (2008) 1358.
[47] F. Zhang, Q. Zhao, L. Kang, D.P. Gaillot, X. Zhao, J. Zhou, D. Lippens, Appl. Phys. Lett. 92 (2008) 193104.